Polariton-Based Quantum Memristors

Ariel Norambuena,[1,*] Felipe Torres,[2,3,4] Massimiliano Di Ventra,[4] and Raúl Coto[1]

[1] *Centro de Investigación DAiTA Lab, Facultad de Estudios Interdisciplinarios, Universidad Mayor 7560908, Chile*

[2] *Center for the Development of Nanoscience and Nanotechnology, Estación Central, Santiago 9170124, Chile*

[3] *Departamento de Física, Facultad de Ciencias, Universidad de Chile, Casilla 653, Santiago 7800024, Chile*

[4] *Department of Physics, University of California, San Diego, La Jolla, California 92093, USA*

(Received 13 September 2021; revised 28 December 2021; accepted 24 January 2022; published 22 February 2022)

Information processing and storage by the same physical system is emerging as a promising alternative to traditional computing platforms. In turn, this requires the realization of elementary units the memory content of which can be easily tuned and controlled. Here, we introduce a polariton-based quantum memristor where the memristive nature arises from the intercavity polariton exchange and is controlled by a time-varying atom-cavity detuning. A dynamical hysteresis is characterized by the fluctuations in the instantaneous polariton number, where the history information is encoded into a dynamical phase. Using a Lindblad master-equation approach, we find that features of the quantum memristor dynamics, such as the area and circulation of the hysteresis loop, showcase a kind of "plasticity" controlled by quantum state initialization. This makes this quantum memristor very versatile for a wide range of applications.

DOI: 10.1103/PhysRevApplied.17.024056

I. INTRODUCTION

Computing in and with memory [1] is emerging as an alternative to our traditional model of computation, which separates the tasks of storage and processing of information into two physically distinct units. Memory (time nonlocality) can be realized in many ways and with different types of systems and devices (for a review, see, e.g., Ref. [2]). However, so far particular attention has been mainly given to *classical* resistive memories (sometimes called "memristive elements") as components of processors with memory [3]. On the other hand, quantum dynamics may offer additional benefits for the realization of storage and information processing capabilities with applications in quantum information and (neuromorphic) quantum computing [4–9].

In this respect, initial suggestions of quantum memristive elements have ranged from superconducting quantum circuits [4–6,10,11] to quantum photonic devices [12]. In all these cases, the memory mechanism arises from the combination of quantum feedback [4,6] and dissipative effects [12]. However, one can also rely on quasiparticle dynamics, such as low-energy quasiparticle tunneling [6] and exciton-polariton interactions [13], as other types of quantum features that can be harnessed to realize quantum memristors.

Among quasiparticles, those originating from strongly correlated light-matter systems, known as polaritons, offer attractive technological features such as room-temperature operation, high dynamical speed, and suitable implementation [14,15]. Polaritons have been implemented in a wide variety of systems, including atoms [16], excitons [17], trapped ions [18], and superconducting circuits [19] and have allowed the observation of quantum phases [20–23].

Recently, more versatile polariton systems have been designed by considering driving schemes [24,25]. The external driving sets a different time scale. Thereby, the time evolution of the system is governed by the difference between the intrinsic response time scale of the system and the driving time scale, leading to bistability. Bistability is a hallmark of driven nonlinear classical and quantum systems [26–31]. In the latter, this is due to the presence of two stable branches where quantum fluctuations switch the states of the system between these two stable solutions [31, 32]. Furthermore, the endeavors to address the response of a system under the influence of an external driving focusing on understanding the out-of-equilibrium dynamics have opened interesting perspectives. Along similar lines, recent works have developed the control of Mott-insulator and superfluid states [33] and the appearance of dynamical hysteresis in photonic devices [31,34].

In this work, we introduce a polariton-based quantum memristor (PQM) the behavior of which is controlled by a time-dependent atomic modulation, providing a hysteretic response over the variance of the number

*ariel.norambuena@umayor.cl

of quasiparticles. The underlying mechanism relies on the intercavity polariton exchange (hopping) and atomic modulation. We demonstrate that memory effects in our PQM depend on the initialization of the system (plasticity) and the time scale of the driving. This minimalistic setup exploits the intercavity polariton exchange, leading to interesting phenomena in more complex optical arrays.

II. POLARITON-BASED QUANTUM MEMRISTOR

The envisioned structure consists of two interacting optical cavities driven by a time-dependent atomic modulation $\xi(t)$. Figure 1 shows a schematic representation of the PQM composed of two cavities doped with a two-level system (which we label φ_g and φ_e), where the intracavity light-matter coupling allows the generation of cavity quantum electrodynamics (QED) polariton quasiparticles and the photon hopping between cavities leads to polariton exchange. Dissipative effects arise from imperfect mirrors with photonic decay (γ_i^c) and spontaneous emission with atomic decay (γ_i^a) per site ($i = 1, 2$). The modulation serves different purposes, such as manipulation of qubits [33,35], sideband transitions [36], and control of atomic quantum gases [37]. The dynamics of the light-matter interaction are given by the Jaynes-Cummings-Hubbard (JCH) Hamiltonian [33],

$$H_0 = \sum_{i=1}^{2}\left[\omega^c a_i^\dagger a_i + \omega^a \sigma_i^\dagger \sigma_i + g\left(a_i\sigma_i^\dagger + a_i^\dagger\sigma_i\right)\right] - J\left(a_1 a_2^\dagger + a_2^\dagger a_1\right), \tag{1}$$

where $\sigma_i = |\varphi_e\rangle_i\langle\varphi_g|_i$ is the raising operator for the two-level atom at the ith cavity, $a_i^\dagger$ and a_i are photon creation and annihilation operators, respectively, ω^c (ω^a) is the cavity (atom) frequency, g is the atom-field coupling strength, and J is the photon hopping strength between neighboring cavities. In this work, we set $\omega^c = \omega^a$ unless stated otherwise. The total Hamiltonian of the system is modeled as

$$H(t) = H_0 + \xi(t)\sum_{i=1}^{2}\sigma_i^\dagger\sigma_i. \tag{2}$$

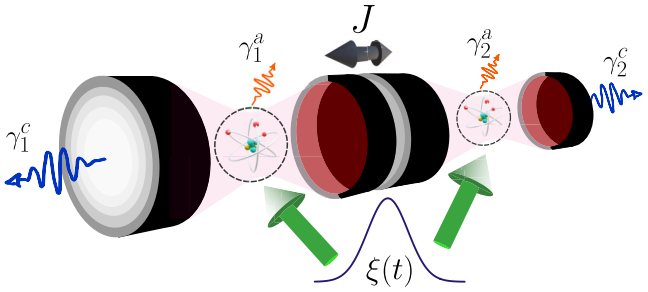

FIG. 1. A schematic representation of the polariton-based quantum memristor composed of two coupled QED cavities with atomic modulation $\xi(t)$. Each cavity interacts with a two-level atom and photon hopping is allowed between the cavities with coupling strength J. Furthermore, each cavity experiences atomic γ_i^a and photonic γ_i^c losses.

We investigate the dynamics induced by a Gaussian modulation given by

$$\xi(t) = \xi_i + (\xi_f - \xi_i)e^{-(t-T)^2/2\sigma_w^2}, \tag{3}$$

where $\xi_f > \xi_i > 0$ and σ_w is the characteristic width of the Gaussian modulation. We explore the dynamics in the regime $\exp[-T^2/(2\sigma_w^2)] \ll 1$, leading to a Gaussian profile satisfying $\xi(0) = \xi(2T) \approx \xi_i$. We introduce the instantaneous polaritonic basis $|n+\rangle = \sin\theta_n(t)|n,\varphi_g\rangle + \cos\theta_n(t)|n-1,\varphi_e\rangle$ and $|n-\rangle = \cos\theta_n(t)|n,\varphi_g\rangle - \sin\theta_n(t)|n-1,\varphi_e\rangle$, with $\theta_n(t) = (1/2)\tan^{-1}[2\sqrt{n}g/\xi(t)]$ and instantaneous eigenenergies $E_{n\pm}(t) = \omega^c n + \xi(t)/2 \pm [\xi^2(t) + 4g^2 n]^{1/2}/2$, where n is the number of photons per cavity. Moreover, sudden interbranch transitions could be activated if $\xi(t)$ has some nonadiabatic features (for further details, see the Supplemental Material [38]).

When the atomic and photonic frequencies are similar, this system exhibits a Mott phase characterized by localized excitations caused by the photon-blockade effect. In this scenario, the effective repulsion between the excitations [16,39] prevents fluctuations of the total number of polaritonic excitations $\sum_i N_i$, where $N_i = a_i^\dagger a_i + \sigma_i^\dagger\sigma_i$ the number of quantum excitations in the ith cavity. A photonic superfluid phase, characterized by delocalized excitations, emerges from the detuning between atomic and photonic frequencies and resembles the flow of charge in a classical resistive memory. During the Mott-superfluid phase transition, the delocalization of the excitations and the polariton exchange lead to an effective quasiparticle flow throughout the optical cavities. In our system, time nonlocality arises from the atomic modulation and memory effects are studied using the variance in the polariton number $\mathrm{var}[N_i(t)] = \mathrm{Tr}\left[N_i^2\rho(t)\right] - \mathrm{Tr}\left[N_i\rho(t)\right]^2$.

We describe the open dynamics using the Markovian master equation $\dot\rho = -i[H(t),\rho] + \mathcal{D}\rho$, where losses are modeled using the Lindblad form [33]:

$$\mathcal{D}\rho = \sum_{i=1}^{2}\left[\gamma_i^c a_i\rho a_i^\dagger + \gamma_i^a\sigma_i\rho\sigma_i^\dagger - \frac{1}{2}\left(\gamma_i^c a_i^\dagger a_i + \gamma_i^a\sigma_i^\dagger\sigma_i,\rho\right)\right]. \tag{4}$$

For concreteness, we first consider an initial Mott-insulator-like state $|\Psi(0)\rangle = |1-\rangle^{\xi(0)} \otimes |1-\rangle^{\xi(0)}$, where $|1-\rangle^{\xi(0)}$ means that the initial state is calculated for $\xi(0)$. Additionally, we set $\xi(t) \geq 10g$ in Eq. (3), which serves two purposes. First, it enables intercavity polariton exchange by suppressing the photon blockade. Second,

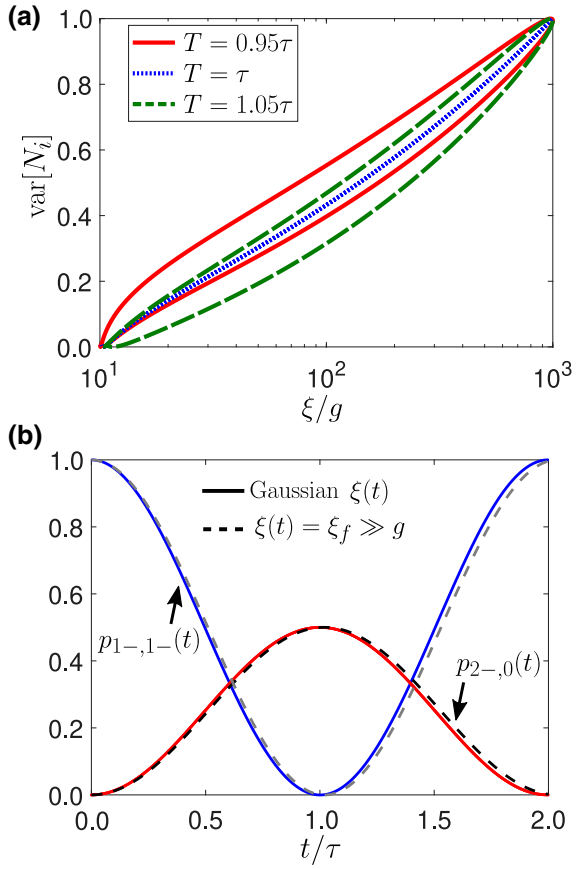

FIG. 2. (a) Dynamical hysteresis curves for a closed PQM with $g = 1$, $J = 10^{-2}g$, $\xi_i = 10g$, $\xi_f = 10^3 g$, $\sigma_w = T/4$, $\omega^c = 10^4 g$, and three different times T in the Gaussian modulation. The initial state is a Mott-insulator-like state $|\Psi(0)\rangle = |1-\rangle \otimes |1-\rangle$ for $\xi(t=0) = \xi_i$. (b) The population dynamics. The solid and dashed lines correspond to the exact and numerical solutions for the Gaussian time-dependent detuning and a large constant detuning, respectively. The case $\xi(t) = \xi_f \gg g$ shows differences with the time-dependent case, since dynamical phases introduce a small shift in the populations.

variations on $\theta_n(t)$ are small, constraining the effect of the modulation to small shifts on the variance. In Fig. 2(a), we show that the evolution of var$[N_i(t)]$ describes a hysteresis loop as a function of $\xi(t)$. We remark that the Mott-superfluid transition takes place regardless of the instantaneous value of $\xi(t)$. However, the driving time scale originates a shift in the population, which can be observed in Fig. 2(b) and in Eqs. (S11) and (S12) in the Supplemental Material [38]. Therefore, as the position of the Gaussian peak (T) changes, different loops appear but there is a critical value [$\tau = \pi/(4J) \approx 78.5g^{-1}$ for $J = 10^{-2}g$] that suppresses the hysteretic behavior (for the estimation of the critical time, see the Supplemental Material [38]). To understand this, we provide a simple argument based on the time symmetry of the functions involved.

Let us consider the time evolution of the occupation probabilities depicted in Fig. 2(b). Throughout the paper, we refer to the occupation probability for each instantaneous two-body polaritonic state $|n\pm, m\pm\rangle$ as $p_{n\pm,m\pm} = \langle n\pm, m\pm|\rho(t)|n\pm, m\pm\rangle$. It is worth noting that there is a characteristic time (τ) that corresponds to the condition $p_{1-,1-}(\tau) = 0$, where the system is in a superfluidlike state, i.e., only states $|2-, 0g\rangle$ and $|2-, 0g\rangle$ (with the same probabilities) are present. Around this time (τ) the dynamics is roughly time symmetric: var$[N_i(\tau + t)] \approx$ var$[N_i(\tau - t)]$. Moreover, the detuning in Eq. (3) is a Gaussian function and it is symmetric around T. Hence, when $T = \tau$, var$[N_i(t)]$ and $\xi(t)$ exhibit the same time symmetry, which makes the hysteresis loop vanish [see Fig. 2(a)]. However, as τ and T differ, the hysteresis loop is restored. The hysteresis loop arises from the delay between the driving time (T) and the time scale of the system (τ). This implies that the irreversibility of the dynamical process is produced by the response time scale of the system against external driving. We analyze the hysteresis-loop area and its circulation for different initial conditions in the closed and open dynamics. In the Supplemental Material [38], we analyze the characteristic time τ in an effective spin-1 system that mimics our PQM.

III. HYSTERESIS-LOOP AREA AND CIRCULATION

The oriented area of a simple connected curve $[x(t), y(t)]$ can be defined as $-\oint y dx$. In our particular case, we have $x(t) = \xi(t)$ (control) and $y(t) =$ var$[N_i]$ (response). The enclosed area in the absence of dissipation is approximately given by

$$A \approx \frac{\eta}{\sqrt{2}}(\xi_f - \xi_i)\pi^{3/2}\frac{\sigma_w}{\tau}\sin\left(\frac{\pi T}{\tau}\right)e^{-[\pi\sigma_w/(\sqrt{2}\tau)]^2}, \quad (5)$$

where $\eta = 1 - 2$var$[N_i(0)]$ is a factor that depends on the state initialization (see the Supplemental Material [38]). We first notice that $A = 0$ for $T = \tau$ [$\sin(\pi T/\tau) = 0$], which explains why the hysteresis vanishes in Fig. 2(a) (dotted line). When $T \neq \tau$, the sign of A accounts for the direction of the circulation, where $A > 0$ (anticlockwise) and $A < 0$ (clockwise). We analytically find that the sign of the area depends on three factors, namely, the variation $\xi_f - \xi_i$ (which is positive in our work), the ratio T/τ, and the factor η that accounts for state initialization. We show in Fig. 3 that the intercavity polariton exchange and the time-dependent driving $\xi(t)$ induce different responses in the variance of the polariton number var$[N_i]$ depending on the initial state $\rho(0) = |\Psi(0)\rangle\langle\Psi(0)|$.

In Fig. 3(a), we show the case where $\eta = 1$ {var$[N_i(0)] = 0$}, leading to anticlockwise (clockwise) circulation for $T < \tau$ ($T > \tau$). In Fig. 3(c), instead, we show the case $\eta = -1$ {var$[N_i(0)] = 1$}, for which the circulation has been inverted with respect to the previous case. In Figs. 3(b)–3(d), we show the hysteresis for the

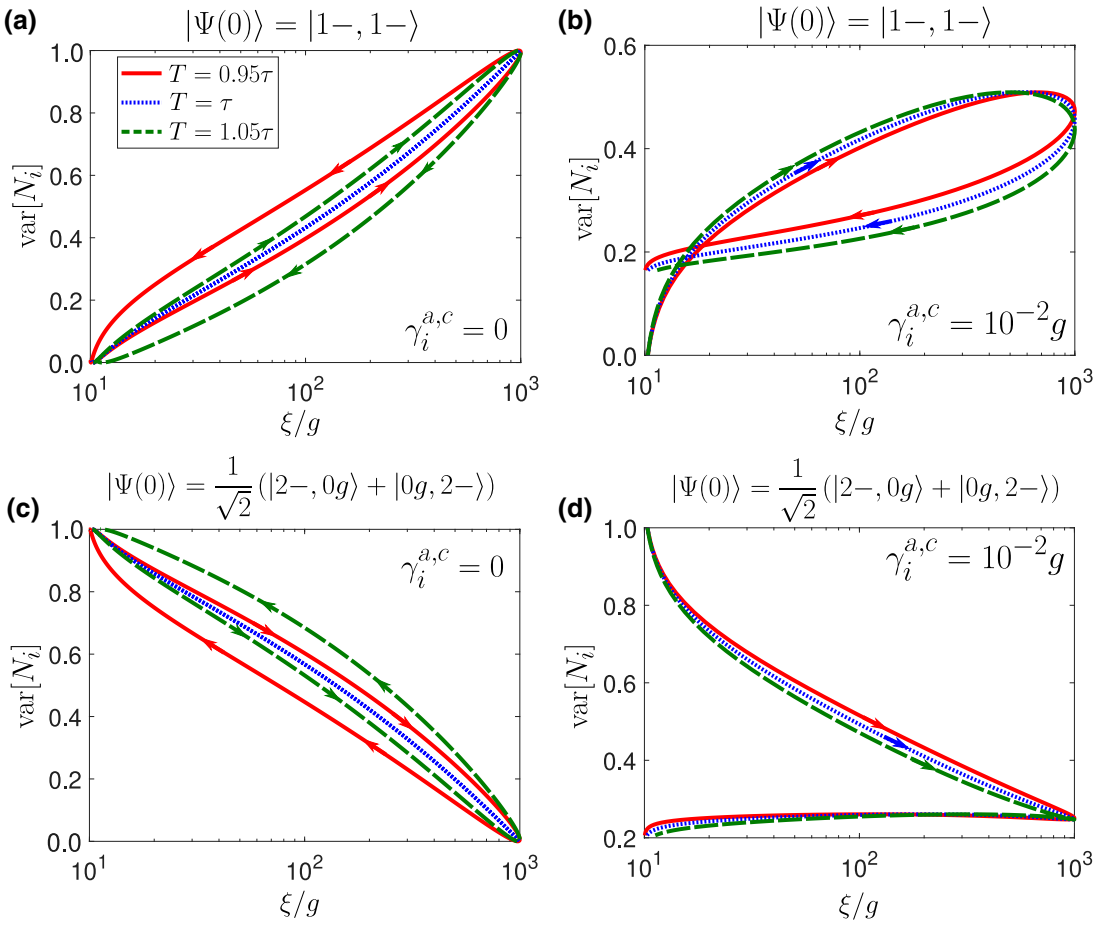

FIG. 3. Hysteresis curves for the Mott-insulator [superfluid] initial condition $|\Psi(0)\rangle = |1-,1-\rangle$ $\{|\Psi(0)\rangle = (1/\sqrt{2})[|2-,0g\rangle + |0g,2-\rangle]\}$ for the closed [(a) and (c)] and open [(b) and (d)] dynamics of the PQM. For all simulations, the parameters are $g = 1$, $J = 10^{-2}g$, $\xi_i = 10g$, $\xi_f = 10^3 g$, $\sigma_w = T/4$, and $\omega^c = 10^4 g$. For the open case, we set $\gamma_i^{a,c} = 10^{-2}g$ for each cavity $i = 1, 2$.

open dynamics. The main difference is that there is still a loop in Fig. 3(b), while in Fig. 3(d), the loop breaks. The latter is a consequence of the initial condition that sets the initial variance $\{\text{var}[N_i(0)]\}$ at the maximum value, while losses do not allow the system to reach that state again. Finally, we remark that the dynamics are no longer symmetric around $\tau = 78.5g^{-1}$; thus the condition $T = \tau$ for shrinking the area fails.

IV. SENSITIVITY TO INITIAL CONDITIONS

Quantum platforms as nonequilibrium photonic systems display dynamics that are subjected to the initial condition. However, the hysteretic behavior seems sometimes insensitive to this, by showing the same loop for different initial states. In order to illustrate this point, we consider two different models, namely the Jaynes-Cummings (JC) and the nonlinear Kerr models. Then, we study the hysteretic behavior as a function of the photonic number [34].

First, we consider the JC model given by a single cavity driven by a continuous wave with frequency ω^p and coupling strength $I(t)$, while the atom is driven with frequency ω^l and Rabi coupling Ω. In a multirotating frame with the atom and cavity frequencies, we obtain

$$H_1(t) = \Delta_a \sigma^\dagger \sigma + \Delta_c a^\dagger a + g\left(a^\dagger \sigma e^{i\Delta_1 t} + a\sigma^\dagger e^{-i\Delta_1 t}\right) + i\Omega(\sigma^\dagger - \sigma) + iI(t)\left(a^\dagger - a\right), \quad (6)$$

where $\Delta_a = \omega^a - \omega^l$, $\Delta_c = \omega^c - \omega^p$, and $\Delta_1 = \omega^p - \omega^l$. Photonic and atomic losses for individual cavities are described by the operator $\mathcal{D}\rho$ defined in Eq. (4). For simplicity, we set $\Omega = 10^{-6}g \ll 1$ and we model $I(t) = I_0 e^{-(t-T)^2/2\sigma_w^2}$ with a Gaussian profile by setting $I_0 = g$, $\sigma = T/4$, and $T = 10^3 g^{-1}$. In Fig. 4(a), we show that the system undergoes a hysteretic behavior for the resonant condition $\Delta_a = \Delta_c = \Delta_1 = 0$ but the loops remain unaffected by the initial conditions.

Second, we consider the driven nonlinear Kerr model, described in Ref. [34], where the system Hamiltonian in the rotating frame at the pumping frequency ω^p is

$$H_{\text{KM}}(t) = -\Delta a^\dagger a + \frac{U}{2}(a^\dagger)^2 a^2 + F(t)(a^\dagger + a), \quad (7)$$

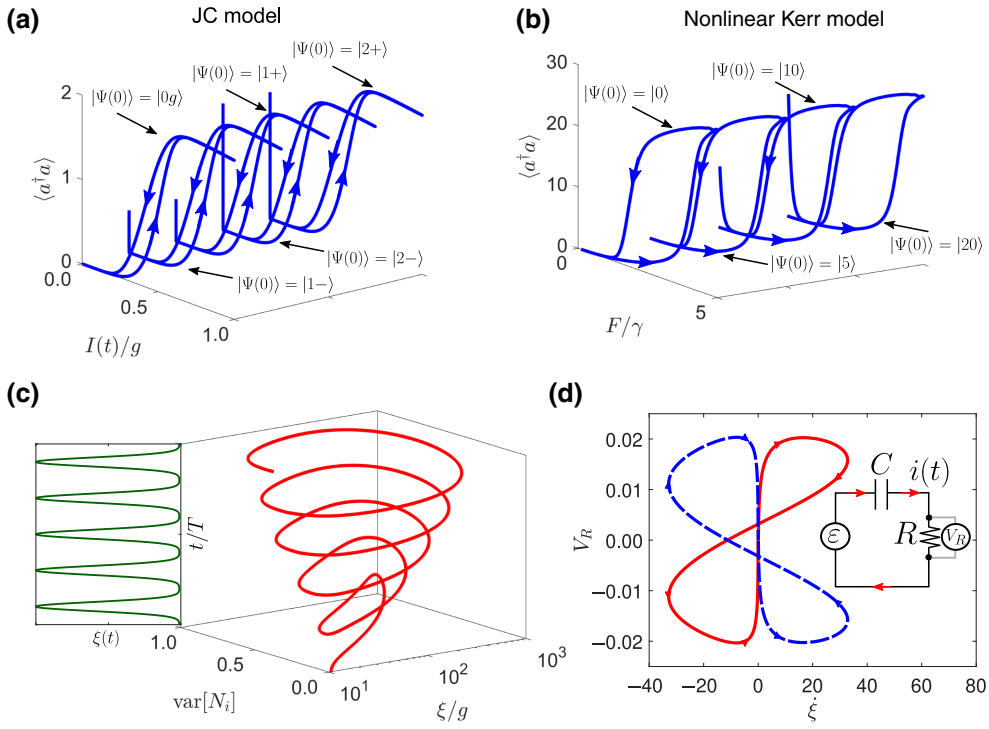

FIG. 4. (a) Hysteresis curves for the Jaynes-Cummings modulated with a time-dependent laser with frequency ω_l and a Gaussian laser amplitude $I(t)$. The hysteresis curves are plotted for the mean number of photons $\langle a^\dagger a\rangle$ as a function of the laser amplitude $I(t)/g$ using different polaritonic initial conditions $|\Psi(0)\rangle$. For the simulation, we use the parameters $g = 1$, $w^a = w^c = w^l = 10^4 g$, $\gamma^a = \gamma^c = g/10$ (photonic and atomic losses) and $T = 0.95\tau$. (b) Hysteresis curves for the nonlinear Kerr model introduced in Ref. [34], with the time-dependent laser amplitude $F(t)$ following a triangular shape with sweep time $t_s = 10\gamma^{-2}\Delta F$, $\Delta F = 3F_0$, $F_0 = \gamma$. The mean number of photons $\langle a^\dagger a\rangle$ as a function of F/γ shows a closed hysteresis loop. For the simulations, we consider $\gamma = 1$, $\Delta = 2\gamma$, $U = 0.1\gamma$, $\gamma = 1$, and different initial Fock states $|\Psi(0)\rangle$. (c) The periodic modulation $\xi(t)$ and its effects on the hysteresis curve $\{\xi(t)/g, \mathrm{var}[N_i]\}$ as a function of time t/T. The three-dimensional plot shows how the response function $\mathrm{var}[N_i]$ describes a spiral when the train pulse $\xi(t)$ is introduced. For the simulation, we consider closed dynamics with $g = 1$, $J = 10^{-2}g$, $\omega^c = 10^4 g$, $T = 0.95\tau$, $\sigma_w = T/4$, and the initial condition $|\Psi(0)\rangle = |1-, 1-\rangle$. (d) The PQM dynamics simulated from Eq. (9) starting from the initial conditions $|\Psi(0)\rangle = |1-, 1-\rangle$ (solid line) and $|\Psi(0)\rangle = (|2-, 0g\rangle + |0g, 2-\rangle)/\sqrt{2}$. The inset shows the PQM circuit analogy, given in Eqs. (9) and (12). For the simulations, we use the parameters $g = 1$, $J = 10^{-2}g$, $\xi_i = 10g$, $\xi_f = 10^3 g$, $\sigma = T/4$, and $\omega^c = 10^4 g$, and $\gamma_i^{a,c} = 0$ for each cavity $i = 1, 2$.

where $\Delta = \omega^p - \omega^a$ and $F(t) = F_0 + (t/t_s)\Delta F\theta(t_s - t) - (t - 2t_s)/t_s\Delta F\theta(t - t_s)$ represent a triangular shape, with ΔF the maximum and $\theta(t)$ the Heaviside step function. For simulating the nonlinear Kerr model, we use the master equation $\dot{\rho} = -i[H_{\mathrm{KM}}(t), \rho] + \gamma/2(2a\rho a^\dagger - \{a^\dagger a, \rho\})$. Once again, we observe dynamical hysteresis without a dependency on the initial conditions [see Fig. 4(b)].

In contrast to the above models, our PQM exhibits hysteresis loops that are sensitive to the initial condition. To shed more light on this, we follow a dynamical approach where we consider a pulse train for the external modulation $\xi(t)$. After each pulse, the system accumulates a phase due to the shifts in the population [see Fig. 2(b)] and ends in a different state, which serves as the initial condition for the incoming pulse. Henceforth, we find in Fig. 4(c) a spiral time-dependent hysteresis loop. We use the term *plasticity* to denote this particular dynamical sensitivity to initial states in our scheme.

Having demonstrated the notion of plasticity, a natural question arises: can our model be mathematically connected with the underlying physics of circuit elements with memory? In particular, this will be useful for physical implementations of quantum neuromorphic computing [4,7] that simulate artificial or biological neural networks.

V. CIRCUIT ANALOGY

In classical resistive memories [2], the current-voltage (I-V) relation $I(t) = G(x(t), V(t), t)V(t)$ holds, where G is the memory conductance and the internal state variables $x(t)$ track the past state history of the system according to the applied input signal. The inclusion of an updating function $\dot{x}(t) = f[x(t), V(t), t]$ typically yields nonlinear dynamics under periodic driving and produces an I-V hysteresis loop [2]. To make a connection between the above circuit elements and our PQM, we use the time-dependent variation of the polariton variance and the Lindblad master

equation to obtain

$$\frac{dy}{d\xi}\dot{\xi} + b(\xi,\rho,t)\xi(t) = a(t,\xi,\rho,t), \tag{8}$$

where $y(t) = \mathrm{Re}\{\mathrm{var}[N_i]\}$ accounts for the real part of the response function and $a(t,\xi,\rho,t) = \mathrm{Re}\{-i\langle[\alpha_i, H_0]\rangle + \mathrm{Tr}[\alpha_i \mathcal{D}\rho]\}$ and $b(t) = \mathrm{Re}\{i\langle[\alpha_i, H_i]\rangle\}$ are dynamical functions that depend on the input function $\xi(t)$, the state of the system $\rho(t)$, and the Hamiltonians H_0 and $H_i = \sum_i \sigma_i^\dagger \sigma_i$. Here, $\alpha_i = (N_i - \langle N_i\rangle)^2 - \langle N_i\rangle^2$, with $\langle N_i\rangle = \mathrm{Tr}(N_i\rho)$. We note that the form of the dynamical system given in Eq. (8) resembles a forced RC circuit, where the following analogies can be recognized: $i(t) \to \dot{\xi}$ (current), $R \to dy/d\xi$ (resistance), $C \to b$ (capacitance), and $\varepsilon \to a$ (voltage) [see Fig. 4(d)]. If we define $R(\xi,\rho,t) = dy/d\xi$ [$C(\xi,\rho,t) = b(\xi,\rho,t)$] as the *differential resistance* (*differential capacitance*), we obtain the following memristive system (with a small memcapacitance in series):

$$V_R = R(\xi,\rho,t)\dot{\xi}, \tag{9}$$

$$V_C = C(\xi,\rho,t)\xi, \tag{10}$$

$$V_R + V_C = a(t,\xi,\rho,t), \tag{11}$$

$$\dot{\rho} = f(\rho,\xi,t). \tag{12}$$

As shown in Fig. 4(d), the above system mimics the dynamics of a current-controlled memristive system [4], where the voltagelike $V_R = \dot{y}$ varies as a function of the current $\dot{\xi}$ and the internal state evolves following a Markovian model $f(\rho,\xi,t) = -i[H(t),\rho] + \mathcal{D}\rho$. We remark that $R(\xi,\rho,t) = dy/d\xi$ can be positive, zero, or even negative and such behavior is connected with the initial condition and the relative time $\tau - T$. For instance, as shown in Fig. 3(a) for $T = 0.95\tau$, the variance starts from $y(t = 0) = 0$ and increases as a function of the detuning ξ, which implies that initially $R(\xi,\rho,t) = dy/d\xi > 0$. On the contrary, in Fig. 3(c) for $T = 0.95\tau$, the initial value is $y(t = 0) = 1$ and the variance decreases in terms of ξ; thus $R(\xi,\rho,t) = dy/d\xi < 0$.

As an example, let us consider two initial conditions $|\Psi(0)\rangle = |1-,1-\rangle$ (solid line with resistance R_1) and $|\Psi(0)\rangle = (|2-,0g\rangle + |0g,2-\rangle)/\sqrt{2}$ (dashed line with resistance R_2). In both cases, we have $V_R(t = 0) = 0$ and $\gamma_i^{a,c} = 0$ $(i = 1,2)$. The simulations illustrated in Fig. 4(d) show two pinched hysteresis loops for the voltage V_R as a function of the current $\dot{\xi}$, where both curves phenomenologically describe the memristive element physics. Finally, we numerically corroborate that the only difference between the two curves in Fig. 4(d) is the sign of the resistances, i.e., $R_1 = -R_2$, which explains the asymmetrical aspect. Finally, there have been a few suggestions of quantum memristors. We remark that the pinched hysteresis loops do not cross the point $(0,0)$, since our model is not a perfect memristive device, as illustrated in Eqs. (9)–(12). In Table I, we report a comparative analysis between currently proposed implementations. The PQM presented here shares some features with superconducting circuits, in the sense that both use quasiparticle manipulation while offering remarkable tunability. In what follows, we provide a framework for designing PQM with quantum technologies.

Quantum dots in a semiconductor microcavity [41] and a photonic crystal nanocavity [42] provide a test bed for quantum technologies. This light-matter interaction has enabled the study of exciton-polaritons [14,43], in close connection to our cavity-QED polaritons; for instance, see Refs. [42,43] for realization of the Jaynes-Cummings model and Ref. [34] for cavity hopping. The parameters for this setup can be accommodated in a wide range. According to Refs. [41,44], the cavity frequency can be tuned around few electronvolts (1.31 eV), while the coupling strength amounts to $g = 80$ μeV (strong coupling) for $Q = 8800$. The hopping strength can be tuned by changing the distance between the micropillars [45] and therefore one could achieve $J = 10^{-2}g$.

Superconducting circuits are at the forefront of quantum computing. Here, a superconducting two-level system that plays the role of an artificial atom interacts with the electric field in a transmission line. Then, one

TABLE I. Characteristics of different types of quantum memristors.

System	Mechanisms	Features	Implementation status
Cavity-QED polariton	Delocalization due to polariton exchange and external driving	Sensitivity to initial states, controlled memory effect without training, and robust behavior against dissipative effects	Theoretical
Beam splitter with a tunable reflectivity [5]	Classical feedback	Resistive memory and fast update speed	Experimental
Superconducting circuits	Quantum feedback [4] or quasiparticle tunneling [6]	Sensitivity to system initialization [6], low-temperature management, and training	Theoretical
Double quantum dot [40]	Capacitive coupling	Low-temperature management and small tunnel barrier	Experimental

can reproduce the Jaynes-Cumming model in the strong coupling regime, where polaritons can be observed and coherently controlled [46,47]. Circuit QED arrays modeled by the Jaynes-Cummings-Hubbard Hamiltonian have been addressed [48,49] and, according to Ref. [49] and the references therein, the parameters can be tuned to the resonator and qubit frequency of few gigahertz (say, 10 GHz), $g = 1$ MHz, and $J = 10^{-2}g$.

VI. CONCLUSIONS

We propose a PQM, where the memristive behavior arises from the intercavity polariton exchange and is controlled by the time-varying atom-cavity detuning (atomic modulation). The hysteresis-loop area and circulation depend on the quantum state initialization and time scales between the system and modulation. This behavior emulates a sort of "plasticity of memristive devices." Remarkably, this plasticity is not observed in hysteretic systems such as the single Jaynes-Cummings and nonlinear Kerr model. This suggests that quasiparticle dynamics offer additional functionalities. From a technical point of view, the implementation of an elementary cavity-QED polariton quantum memristor, the memory content of which is controlled by the state initialization, adds interesting features such as room-temperature operation and high dynamical speed. However, perhaps the most significant aspect of PQMs, as opposed to classical memristive elements, may be the energy-efficient flow of quasiparticles, which does not involve thermal dissipation due to the Joule heating. This essential feature is crucial for low-energy applications and it makes the PQM an exciting and versatile candidate for the use of strongly correlated light-matter systems in the field of memcomputing and (neuromorphic) quantum computation.

ACKNOWLEDGMENTS

The authors thank Peter Rabl, Gabriel Alvarado, and Francisco Albarrán-Arriagada for helpful insights and comments on the manuscript. A.N. acknowledges financial support from Universidad Mayor through the Postdoctoral Fellowship. R. C. acknowledges financial support from Fondecyt Iniciación No. 11180143. F. T. acknowledges financial support from Fondo Nacional de Investigaciones Científicas y Tecnológicas (FONDECYT, Chile) under grants 1211902, Centro de Nanociencia y Nanotecnología CEDENNA, Financiamiento Basal para Centros Científicos y Tecnológicos de Excelencia AFB180001, and Beca Santander Movilidad Internacional Profesores. M. D. acknowledges financial support from the Department of Energy under Grant No. DE-SC0020892.

A.N. and R.C. created the theoretical model. F.T. conceived the connection with memristive elements and M.D. realized insightful comments and observations related to memristor physics. A.N. performed all the numerical simulations. All of the authors prepared, proofread, commented on, and approved the manuscript.

M.D. is the co-founder of MemComputing, Inc. [50], which is attempting to commercialize the memcomputing technology. All other authors declare no competing interests.

[1] M. Di Ventra and Y. V. Pershin, The parallel approach, Nat. Phys. **9**, 200 (2013).
[2] Y. V. Pershin and M. Di Ventra, Memory effects in complex materials and nanoscale systems, Adv. Phys. **60**, 145 (2011).
[3] F. L. Traversa and M. Di Ventra, Universal memcomputing machines, IEEE Trans. Neural Netw. Learn. Syst. **26**, 2702 (2015).
[4] P. Pfeiffer, I. L. Egusquiza, M. Di Ventra, M. Sanz, and E. Solano, Quantum memristors, Sci. Rep. **6**, 29507 (2016).
[5] L. C. Céleri, T. Gonzalez-Raya, J. M. Lukens, and M. Sanz, Quantum memristors in frequency-entangled optical fields, Materials **13**, 864 (2020).
[6] J. Salmilehto, F. Deppe, M. Di Ventra, M. Sanz, and M. E. Solano, Quantum memristors with superconducting circuits, Sci. Rep. **7**, 42044 (2017).
[7] D. Marković and J. Grollier, Quantum neuromorphic computing, Appl. Phys. Lett. **117**, 150501 (2020).
[8] S. N. Shevchenko, Y. V. Pershin, and F. Nori, Qubit-Based Memcapacitors and Meminductors, Phys. Rev. Appl. **6**, 014006 (2016).
[9] S. N. Shevchenko and D. S. Karpov, Thermometry and Memcapacitance with a Qubit-Resonator System, Phys. Rev. Appl. **10**, 014013 (2018).
[10] S. Kumar, F. A. Cardenas-Lopez, N. N. Hegade, X. Chen, F. Albarran-Arriagada, E. Solano, and G. A. Barrios, Entangled quantum memristors, Phys. Rev. A **104**, 062605 (2021).
[11] S. Peotta and M. Di Ventra, Superconducting Memristors, Phys. Rev. Appl. **2**, 034011 (2014).
[12] M. Sanz, E. Solano, and L. Lamata, Invited article: Quantum memristors in quantum photonics, APL Photonics **3**, 080801 (2018).
[13] R. Mirek, A. Opala, P. Comaron, M. Furman, M. Król, K. Tyszka, B. Seredyński, D. Ballarini, D. Sanvitto, T. C. H. Liew, *et al.*, Neuromorphic binarized polariton networks, Nano Lett. **21**, 3715 (2021).
[14] T. Boulier, M. J. Jacquet, A. Maître, G. Lerario, F. Claude, S. Pigeon, Q. Glorieux, A. Amo, J. Bloch, A. Bramati, and E. Giacobino, Microcavity polaritons for quantum simulation, Adv. Quantum Technol. **3**, 2000052 (2020).
[15] D. N. Basov, A. Asenjo-Garcia, P. J. Schuck, X. Zhu, and A. Rubio, Polariton panorama, Nanophotonics **10**, 549 (2021).
[16] K. M. Birnbaum, A. Boca, R. Miller, A. D. Boozer, T. E. Northup, and H. J. Kimble, Photon blockade in an optical cavity with one trapped atom, Nature **436**, 87 (2005).
[17] C. Weisbuch, M. Nishioka, A. Ishikawa, and Y. Arakawa, Observation of the Coupled Exciton-Photon Mode Splitting

in a Semiconductor Quantum Microcavity, Phys. Rev. Lett. **69**, 3314 (1992).
[18] K. Toyoda, Y. Matsuno, A. Noguchi, S. Haze, and S. Urabe, Experimental Realization of a Quantum Phase Transition of Polaritonic Excitations, Phys. Rev. Lett. **111**, 160501 (2013).
[19] J. Raftery, D. Sadri, S. Schmidt, H. E. Türeci, and A. A. Houck, Observation of a Dissipation-Induced Classical to Quantum Transition, Phys. Rev. X **4**, 031043 (2014).
[20] M. J. Hartmann, F. G. S. L. Brandão, and M. B. Plenio, Strongly interacting polaritons in coupled arrays of cavities, Nat. Phys. **2**, 849 (2006).
[21] A. D. Greentree, C. Tahan, J. H. Cole, and L. C. L. Hollenberg, Quantum phase transitions of light, Nat. Phys. **2**, 856 (2006).
[22] M. Fitzpatrick, N. M. Sundaresan, A. C. Y. Li, J. Koch, and A. A. Houck, Observation of a Dissipative Phase Transition in a One-Dimensional Circuit QED Lattice, Phys. Rev. X **7**, 011016 (2017).
[23] J. Kasprzak, M. Richard, S. Kundermann, A. Baas, P. Jeambrun, J. M. J. Keeling, F. M. Marchetti, M. H. Szymańska, R. André, J. L. Staehli, *et al.*, Bose-Einstein condensation of exciton polaritons, Nature **443**, 409 (2006).
[24] L. W. Clark, N. Jia, N. Schine, C. Baum, A. Georgakopoulos, and J. Simon, Interacting Floquet polaritons, Nature **571**, 532 (2019).
[25] P. S. Mundada, A. Gyenis, Z. Huang, J. Koch, and A. A. Houck, Floquet-Engineered Enhancement of Coherence Times in a Driven Fluxonium Qubit, Phys. Rev. Appl. **14**, 054033 (2020).
[26] H. M. Gibbs, S. L. McCall, and T. N. C. Venkatesan, Differential Gain and Bistability Using a Sodium-Filled Fabry-Perot Interferometer, Phys. Rev. Lett. **36**, 1135 (1976).
[27] F. S. Felber and J. H. Marburger, Theory of nonresonant multistable optical devices, Appl. Phys. Lett. **28**, 731 (1976).
[28] L. A. Lugiato, II theory of optical bistability, Prog. Opt. **21**, 69 (1984).
[29] G. Rempe, R. J. Thompson, R. J. Brecha, W. D. Lee, and H. J. Kimble, Optical Bistability and Photon Statistics in Cavity Quantum Electrodynamics, Phys. Rev. Lett. **67**, 1727 (1991).
[30] J. Gripp, S. L. Mielke, L. A. Orozco, and H. J. Carmichael, Anharmonicity of the vacuum Rabi peaks in a many-atom system, Phys. Rev. A **54**, R3746(R) (1996).
[31] S. R. K. Rodriguez, W. Casteels, F. Storme, N. C. Zambon, I. Sagnes, L. L. Gratiet, E. Galopin, A. Lemaître, A. Amo, C. Ciuti, and J. Bloch, Probing a Dissipative Phase Transition via Dynamical Optical Hysteresis, Phys. Rev. Lett. **118**, 247402 (2017). R3746(R).
[32] D. Huybrechts and M. Wouters, Dynamical hysteresis properties of the driven-dissipative Bose-Hubbard model with a Gutzwiller Monte Carlo approach, Phys. Rev. A **102**, 053706 (2020).
[33] D. Tancara, A. Norambuena, R. Peña, G. Romero, F. Torres, and Raúl Coto, Steering interchange of polariton branches via coherent and incoherent dynamics, Phys. Rev. A **103**, 053708 (2021).
[34] W. Casteels, F. Storme, A. Le Boité, and C. Ciuti, Power laws in the dynamic hysteresis of quantum nonlinear photonic resonators, Phys. Rev. A **93**, 033824 (2016).
[35] J. D. Strand, M. Ware, F. Beaudoin, T. A. Ohki, B. R. Johnson, A. Blais, and B. L. T. Plourde, First-order sideband transitions with flux-driven asymmetric transmon qubits, Phys. Rev. B **87**, 220505(R) (2013).
[36] F. Beaudoin, M. P. da Silva, Z. Dutton, and A. Blais, First-order sidebands in circuit QED using qubit frequency modulation, Phys. Rev. A **86**, 022305 (2012).
[37] A. Eckardt, Colloquium: Atomic quantum gases in periodically driven optical lattices, Rev. Mod. Phys. **89**, 011004 (2017).
[38] See the Supplemental Material at http://link.aps.org/supplemental/10.1103/PhysRevApplied.17.024056 for further details of the model such as the spin-1 representation, approximated solutions, derivations of the area formula and numerical details of the simulation in the non-adiabatic case.
[39] D. G. Angelakis, M. F. Santos, and S. Bose, Photon-blockade-induced Mott transitions and *xy* spin models in coupled cavity arrays, Phys. Rev. A **76**, 031805(R) (2007).
[40] Y. Li, G. W. Holloway, S. C. Benjamin, G. A. D. Briggs, J. Baugh, and J. A. Mol, Double quantum dot memristor, Phys. Rev. B **96**, 075446 (2017).
[41] J. P. Reithmaier, G. Sek, A. Löffler, C. Hofmann, S. Kuhn, S. Reitzenstein, L. V. Keldysh, V. D. Kulakovskii, T. L. Reinecke, and A. Forchel, Strong coupling in a single quantum dot-semiconductor microcavity system, Nature **432**, 197 (2004).
[42] K. Kuruma, Y. Ota, M. Kakuda, S. Iwamoto, and Y. Arakawa, Time-resolved vacuum Rabi oscillations in a quantum-dot-nanocavity system, Phys. Rev. B **97**, 235448 (2018).
[43] T. Neuman and J. Aizpurua, Origin of the asymmetric light emission from molecular exciton-polaritons, Optica **5**, 1247 (2018).
[44] S. M. de Vasconcellos, A. Calvar, A. Dousse, J. Suffczyński, N. Dupuis, A. Lemaître, I. Sagnes, J. Bloch, P. Voisin, and P. Senellart, Spatial, spectral, and polarization properties of coupled micropillar cavities, Appl. Phys. Lett. **99**, 101103 (2011).
[45] M .Galbiati, L. Ferrier, D. D. Solnyshkov, D. Tanese, E. Wertz, A. Amo, M. Abbarchi, P. Senellart, I. Sagnes, A. Lemaître, E. Galopin, G. Malpuech, and J. Bloch, Polariton Condensation in Photonic Molecules, Phys. Rev. Lett. **108**, 126403 (2012).
[46] A. Wallraff, D. I. Schuster, A. Blais, L. Frunzio, R.-S. Huang, J. Majer, S. Kumar, S. M. Girvin, and R. J. Schoelkopf, Strong coupling of a single photon to a superconducting qubit using circuit quantum electrodynamics, Nature **431**, 162 (2004).
[47] A. Blais, R.-S. Huang, A. Wallraff, S. M. Girvin, and R. J. Schoelkopf, Cavity quantum electrodynamics for superconducting electrical circuits: An architecture for quantum computation, Phys. Rev. A **69**, 062320 (2004).
[48] A. A. Houck, H. E. Türeci, and J. Koch, On-chip quantum simulation with superconducting circuits, Nat. Phys. **8**, 292 (2012).
[49] S. Schmidt and J. Koch, Circuit QED lattices: Towards quantum simulation with superconducting circuits: Circuit QED lattices, Ann. Phys. **525**, 395 (2013).
[50] https://memcpu.com/.